This document is confidential and is proprietary to the American Chemical Society and its authors. Do not copy or disclose without written permission. If you have received this item in error, notify the sender and delete all copies.

Giant Terahertz Birefringence in an Ultrathin Anisotropic Semimetal

Journal: 17	Nano Letters
	nl-2024-00758q.R1
Manuscript Type: 0	Communication
Date Submitted by the Author:	n/a
	Sie, Edbert; Stanford University Othman, Mohamed; SLAC Nyby, Clara; Stanford University, Chemistry Pemmaraju, Das; SLAC Garcia, Christina; Harvard University, John A. Paulson School of Engineering and Applied Sciences Wang, Yaxian; Harvard University, John A. Paulson School of Engineering and Applied Sciences Guzelturk, Burak; Argonne National Laboratory Advanced Photon Source, X-ray Science Division Xia, Chenyi; Stanford University Poletayev, Andrey; University of Oxford, Ofori-Okai, Benjamin; SLAC Hoffmann, Matthias; Stanford University, SLAC National Accelerator Laboratory Park, Suji; SLAC Shen, Xiaozhe; SLAC Yang, Jie; SLAC Li, Renkai; SLAC Reid, Alexander; SLAC National Accelerator Laboratory, SIMES Weathersby, Stephen; SLAC National Accelerator Laboratory Muscher, Philipp; Stanford University Finney, Nathan; Columbia University Rhodes, Daniel; University of Wisconsin-Madison, Material Science and Engineering Balicas, Luis; Florida State University, National High Magnetic Field Laboratory Nanni, Emilio; SLAC Hone, James; Columbia University, Mechanical Engineering Chueh, William; Stanford University, Materials Science & Enginerring; Devereaux, Thomas; Stanford University, Narang, Prineha; UCLA Heinz, Tony; Stanford University Wang, Xijie; SLAC Lindenberg, Aaron; Stanford University, Department of Materials Science and Engineering

SCHOLARONE™ Manuscripts

Giant Terahertz Birefringence in an Ultrathin Anisotropic Semimetal

Authors: Edbert J. Sie^{1,2,†}, Mohamed A. K. Othman^{3,†}, Clara M. Nyby⁴, Das Pemmaraju², Christina A. C. Garcia⁵, Yaxian Wang⁵, Burak Guzelturk⁶, Chenyi Xia⁷, Jun Xiao^{7,8}, Andrey Poletayev⁷, B. K. Ofori-Okai³, Matthias C. Hoffmann³, Su Ji Park², Xiaozhe Shen³, Jie Yang³, Renkai Li³, Alexander H. Reid³, Stephen Weathersby³, Philipp Muscher², Nathan Finney⁹, Daniel Rhodes⁹, Luis Balicas¹⁰, Emilio Nanni³, James Hone¹¹, William Chueh^{2,7}, Thomas P. Devereaux^{3,7}, Prineha Narang¹³, Tony F. Heinz^{2,11,14}, Xijie Wang^{3,15,16}, Aaron M. Lindenberg^{2,7,14,*}

Affiliations:

- ¹ Geballe Laboratory for Advanced Materials, Stanford University, Stanford, CA 94305, USA.
- ² Stanford Institute for Materials and Energy Sciences (SIMES), SLAC National Accelerator Laboratory, Menlo Park, CA 94025, USA.
- ³ SLAC National Accelerator Laboratory, Menlo Park, CA 94025, USA.
- ⁴ Department of Chemistry, Stanford University, Stanford, CA 94305, USA.
- ⁵ John A. Paulson School of Engineering and Applied Sciences, Harvard University, Cambridge MA 02138, USA.
- ⁶ X-ray Science Division, Advanced Photon Source, Argonne National Laboratory, Lemont, Illinois 60439, USA
- ⁷ Department of Materials Science and Engineering, Stanford University, Stanford, CA 94305, USA.
- ⁸ Department of Materials Science and Engineering, University of Wisconsin-Madison, Madison, Wisconsin 53706, USA
- ⁹ Department of Mechanical Engineering, Columbia University, New York, NY 10027, USA.
- ¹⁰ National High Magnetic Field Laboratory and Department of Physics, Florida State University, Tallahassee, FL 32310, USA.
- ¹¹ Department of Mechanical Engineering, Columbia University, New York, NY 10027, USA.
- ¹² Department of Applied Physics, Stanford University, Stanford, CA 94305, USA.
- ¹³ College of Letters and Science, University of California, Los Angeles, CA 90095, USA
- ¹⁴ Stanford PULSE Institute, SLAC National Accelerator Laboratory, Menlo Park, CA 94025, USA.
- ¹⁵ Faculty of Physics, University of Duisburg-Essen, 47057 Duisburg, Germany
- ¹⁶ Department of Physics, University Dortmund, 44221 Dortmund, Germany

†These authors contributed equally

Abstract:

Manipulating the polarization of light at the nanoscale is key to the development of next generation optoelectronic devices. This is typically done via waveplates using optically anisotropic crystals, with thicknesses of order the wavelength. In the terahertz (THz) frequency range, these waveplates have thickness ~1 mm, which makes them bulky and not integrable with on-chip devices. Here, using a novel ultrafast electron-beam-based technique sensitive to transient near fields at THz frequencies, we observed a giant anisotropy in the linear optical response in the semimetal WTe₂,

^{*} Correspondence to: aaronl@stanford.edu

and demonstrated that one can tune the THz polarization using a 50-nanometer thick WTe₂ film, which acts as a broadband THz wave plate with thickness three orders of magnitude smaller than the wavelength. The observed circular deflections of the electron beam are consistent with simulations tracking the trajectory of the electron beam in the near field of the THz pulse. This finding offers a promising approach to enable atomically-thin THz polarization control using anisotropic semimetals and defines new approaches for characterizing THz near field optical response at far-sub-wavelength length-scales.

Keywords: Terahertz, two-dimensional materials, Tungsten ditelluride, waveplate, ultrafast electron diffraction

Main text:

Birefringence is the optical property of a material in which the refractive index depends on the polarization of incident light. It serves as a direct measure of broken symmetry and anisotropy in the structure of materials, and acts as a probe of the novel electronic properties of materials, while simultaneously enabling numerous optoelectronic applications^{1,2}. Birefringent materials are used to alter the polarization of light, either by rotating the angle of polarization or, as in the case of the quarter-wave plate, to convert linearly polarized light into circularly polarized light. Typically, a thickness on the order of the incident wavelength is required to accumulate this phase shift in the birefringent material. For instance, quartz has a birefringence $\Delta n = 0.009$ at wavelength $\lambda = 590$ nm, where Δn is the difference in the index of refraction along principal axes of the material. It becomes a quarter-wave plate with thickness $d = \lambda/(4\Delta n) = 16.4$ µm. At a longer wavelength, $\lambda = 100 \text{ }\mu\text{m}$ ($\Delta n = 0.044$), it requires a significantly larger thickness of d = 0.6 mm to act as a quarter-wave plate. Here, we observed significant changes in the polarization state of a THz pulse, akin to quarter-wave plate behavior, using a WTe₂ crystal only 50-nm thick (thickness $\lambda/2000$). Prior studies have investigated other anisotropic van der Waals semiconductors such as black phosphorus, ReS₂ and ReSe₂, with thickness $\sim \lambda^{3,4}$, quasi-1D semiconductor BaTiS₃ ($\sim \lambda/3$) ⁵, as well as the in-plane hyperbolic α -MoO₃ semiconductor^{6,7} all of which show smaller birefringent responses. Recent efforts have additionally demonstrated novel types of polarization control at optical-near-IR wavelengths using atomically thin van der Waals materials but typically require cavity geometries to enhance the response in this ultrathin limit.^{8,9} The characterization of the photonic properties of these materials in both the near and far field remains poorly developed, especially in the small sample, sub-wavelength limit.

WTe₂ is a layered semimetal with a strongly anisotropic in-plane structure. ¹⁰⁻¹³ The tungsten atoms dimerize along the crystallographic a-axis and form an array of quasi-1D metallic chains. Despite having a structural resemblance to a wire-grid polarizer, the actual optical functionality of WTe₂ is more complex. To study the electrodynamic anisotropy of WTe₂ we used quasi-single cycle broadband THz light pulses with peak field \sim 625 kV/cm and frequency centered at 3 THz sent at normal incidence through a 50-nm thick WTe₂ exfoliated crystal. Conventional means of

characterizing THz polarization via electro-optic sampling or polarized detection of the transmitted light cannot be implemented straightforwardly because of the small lateral size of the sample (110 μ m × 30 μ m) relative to the THz spot size (~1 mm). In our experiments, the deflection of 100 fs relativistic electron bunches is measured to directly probe the THz polarization state in the near field field. This technique can discriminate the THz fields within the sample boundary by selectively probing the diffracted electron beam, even when the incident electron beam and terahertz spot sizes are significantly larger than the sample, thus providing sensitivity to the localized fields within a transversely small sample. The electrons have a relativistic kinetic energy of 3.1 MeV, which is crucial to ensure that the electron bunches travel at nearly the same speed (0.99c) as the THz light pulses, thus enabling measurement of the electric field polarization within the optical cycle of the THz light field. In particular, the electron bunches exhibit a momentum kick along the THz electric field polarization, referred to as THz streaking c0. Thus enabling direct mapping of the THz polarization via measurement of the electron trajectory.

Figure 1a illustrates the trajectory of the electron beam through a pinhole that exhibits THz streaking along the vertical or horizontal electric field direction. The electron beam is detected by a camera located downstream, from which the transverse displacement is measured. Figure 1b shows the experimentally measured streaking at various incident THz polarizations through a pinhole (without WTe₂ sample). The finite pulse duration of the electron bunches and ~100 fs timing jitter resulted in an elongated streaking image, instead of a displaced point-like image, and show the as-expected linear trajectory along the incident THz polarization. This is in contrast to an otherwise undisturbed point-like image in the absence of an applied THz field. Such a fundamental, coherent light-matter interaction should occur not only for linear THz polarization but also for elliptical and circular THz polarizations (Fig. 1c). The effect of THz streaking through WTe2, with the crystallographic axes shown in Fig. 2a-b, is well captured by the electron diffraction pattern from the sample (Fig. 2c-f). In the absence of external fields, the diffraction pattern consisted of a two-dimensional array of point-like Bragg peaks along the crystallographic a and b axes (Fig. 2c). In the presence of THz fields aligned along these axes, however, all of the Bragg peaks exhibited a linear THz streaking, similar to the pinhole case, while preserving the diffraction pattern (Fig. 2d-e). In particular, the electron beam deflected along the vertical and horizontal directions when the incident THz polarization is along the crystallographic a and b axes, respectively. Remarkably, when the THz field is polarized at 45° with respect to the a and b axes - thus sampling the anisotropic index of refraction - every Bragg peak showed a circular trajectory (Fig. 2f), in stark contrast with the linear trajectory expected for isotropic materials (see Supplementary Movies M1-4, showing that all Bragg peaks made this circular motion in a concerted manner only for the case where the THz field samples both a and b axes).

To investigate this unique streaking behavior, we isolated the brightest Bragg peak (200) and monitored the streaking image for various orientations of the linearly polarized incident THz field with respect to the *b*-axis (Fig. 3a). The streaking images show a clear progression from linear to

elliptical to circular trajectories and then back to linear as we rotated the incident THz polarization through 90 degrees. This behavior is identical to that of a quarter-wave plate. Note that the brightest intensity persisted at the center of every image, indicating the fraction of electron bunch (temporal duration ~100 fs) that trailed behind the THz pulse duration (~150 fs for the main cycle), influenced also by the timing jitter between electron and THz pulses. We also found that the streaking diameter increased linearly with THz field at +45°, while preserving a circular trajectory (Fig. 3b-c). This behavior is consistent with a deflection by the Lorentz force $\vec{F} = -e(\vec{E} + \vec{v} \times \vec{B})$ where both the electric and magnetic components of the THz field contribute linearly to the deflection, with opposite sign (see also Supporting Text S1). 15 Conversely, by tracking the electron deflection downstream we deduce the corresponding amplitude and polarization vector of the THz field in a time-resolved manner through the relation $\vec{E}(t) = E_0(\hat{x}\theta_x(t) + \hat{y}\theta_y(t))$, where E_0 (~0.8 MV/cm) is a proportionality constant and $\theta_x(t)$, $\theta_y(t)$ are the time-dependent deflections in milliradians. The linear increase of the deflection with THz field (Fig. 3c) further indicates that the birefringence we observed is a linear optical effect, which is independent of the incident electric field strength. Our observation is consistent with a recent measurement where circularly polarized THz light was prepared in advance and directly sent through a pinhole to deflect a co-propagating electron beam ²⁰.

To determine the handedness of the circular polarization, we studied the electron trajectories through measurement of the streaking snapshots ($+45^{\circ}$) at increasing time delay t between the electron bunch and the THz pulse (Fig. 4a). Note that the snapshots are flipped images of the actual trajectories as seen from the electron beam source due to a folding mirror (after the phosphor screen) downstream to project an image on the camera. In addition, the electron's deflection is opposite to the applied THz electric field due to electron's negative charge in the Lorentz force (Supporting Text S1). Hence, the snapshots in Fig. 4a provide an identical representation of the amplitude and polarization vector of the THz electric field (in the near field). The trajectory started at the center of the image and rotated counter-clockwise, with the loop spanning the upper half of the image. This behavior is consistent with a quasi-single cycle left-circularly polarized THz pulse, with the convention of handedness viewed from the light source. In this way we can assign the handedness of the other THz polarizations depicted in Fig. 3a. That is, we obtained a left-circularly polarized THz pulse using an incident THz field polarized at +45° and +225°, and a right-circularly polarized THz pulse using an incident field polarized at +135° and +315°. This is exactly the condition required to produce circularly polarized light by means of a quarter-wave plate. One can obtain the effective birefringence between the a and b axes through its phase retardation, $\Delta \phi =$ $\frac{2\pi}{\lambda}d\Delta n$ where d is the sample thickness, Δn the effective birefringence, and λ the wavelength. By taking d = 50 nm and $\lambda = 100$ µm (3 THz) to produce an ideal guarter-wave phase retardation $(\Delta \phi = \pi/2)$, we obtained an effective birefringence of $\Delta n = 500$. We note that the response is broadband with no indication of significant stretching of the incident field, as shown in Supporting Fig. S6.

WTe2 is a semimetal and it has a large dielectric function at THz frequencies similar to those in typical metals, e.g. aluminum and gold ($\varepsilon \sim 10^5$) ^{21,22}. However, unlike most metals, WTe₂ is strongly anisotropic because of the spontaneous formation of quasi-1D metallic chains along the a-axis¹⁰ (Fig. 2a). Although in principle the dielectric function has contributions from both electrons and phonons, our ab initio electronic structure calculations (DFT and diagrammatic techniques) and prior experiments showed that the intraband electronic contribution dominates the conductivity at THz frequencies (Supporting Information S4). Hence, the dielectric functions can be approximated using a Drude model. ²³⁻²⁵ In this model, the dielectric function is given by $\varepsilon \approx$ $-\omega_{n,a,b}^2/(\omega^2+i\omega/\tau_{a,b})$, which can be separated into real and imaginary parts, $\varepsilon_1=$ $-\omega_{p,a,b}^2/(\omega^2+1/\tau_{a,b}^2)$ and $\varepsilon_2=(\omega_{p,a,b}^2/\omega\tau_{a,b})/(\omega^2+1/\tau_{a,b}^2)$ where the subscripts a and b define anisotropic values for the plasma frequency and scattering time along the two in-plane crystallographic axes. The distinct Drude behavior along the two axes is apparent from the anisotropy in the electronic band structure, i.e. strongly dispersive along k_a and weakly dispersive along k_b 11, with differing dc/ac-conductivities. The real part of the dielectric functions become very large and negative when approaching 3 THz and show significantly different values for light polarized along a and b axes²³, consistent with the large and broadband birefringence we observed. Supporting Information section S6 provides additional details on the Drude response of the film and estimates the required anisotropic materials parameters required to induce the observed large birefringences within an approximate 2D model for the transmitted field.²⁶ We find significant phase shifts approaching $\pi/3$ even within this simple model using values $\tau_a=100$ fs, $\tau_b=30$ fs, $\omega_{p,a}$ =5800 cm⁻¹, $\omega_{p,b}$ =4000 cm⁻¹, with the anisotropic plasma frequencies consistent with reference 23. Fig. S9 shows the associated frequency dependent dielectric function in a Drude model using these values. Supporting Information section S8 describes ab-initio electronic structure calculations of the anisotropies in the scattering times and other Drude parameters. The ab-initio calculation provides supporting evidence for significant anisotropies of the correct sign in the dielectric constant and in the induced phase shift, but predict somewhat smaller magnitudes in the anisotropic scattering times than experimentally extracted. We note that similar anisotropies in both the scattering times and Drude weights have been recently experimentally reported²⁷. A quantitative model likely requires consideration of contributions beyond the simple Drude model.

To simulate and quantify more accurately the trajectories of the streaked electrons within the THz near field, we used a frequency domain finite-element solver to obtain both the electric and magnetic field 3D distribution and Fourier coefficients that represent the interaction of the THz pulse (with spectral content 0.1-5 THz) with the WTe₂ thin film, including the effects from the SiN window substrate, and using the Drude model parameters given above. We used 30 Fourier coefficients to fully construct the frequency spectrum of the THz pulse. Snapshots of the electric fields in the z-x plane in the vicinity of the sample shows transient behavior the field components and leads to a delay, or phase offset, between the two polarizations, shown in Fig. 4b (more details in Supporting Information S10). Such 3D transient field maps were then used in space-charge

particle tracking code (GPT*) to track the electrons from the UED rf-gun through the sample, downstream to the detector, following previous work¹⁹. The results, shown in Fig. 4c, indicate that the electron trajectories track the polarization of the THz pulse in the near fields of the WTe₂ sample and show results consistent with experiment (Fig. 4a). Figure 4d shows the simulated helical trajectory of the electron beam in the near field of the sample for THz field incident at 45 deg. This behavior is obtained solely from material anisotropy when excited with polarization state at 45° with respect to the in-plane axes. Indeed, a film with isotropic properties only shows linear streaking (Fig. 4e) proving that the material anisotropy plays a key role in the THz transmission and the near field response. Additionally, similar calculations in the large transverse film limit show that these effects are not arising solely from edge effects which play a small role in the near field birefringence (Supporting Information S10).

The semimetal nature of this material renders the absorption coefficient to be larger than those found in typical birefringent materials but still corresponds to a rather high transmission coefficient in this nanoscale limit. We estimated using the best fit dielectric constant values from the experiment and in a 2d model for the complex transmission coefficient (equation S3) values of order 20% for the THz field for a 50 nm film. So while somewhat lossy, this shows a reasonably high transparency for nanoscale film thicknesses. Additional measurements described in Supporting Information S7 show tabletop THz transmission measurements with thicker WTe₂ samples and compare to other isotropic systems, supporting these estimates.

In conclusion, we observed a giant birefringence in the anisotropic semimetal WTe₂ by characterizing the THz polarization state in the near field through the deflection of femtosecond diffracted electrons. Such a large birefringence arises from the strongly anisotropic structure of WTe₂ as the metallic W ions dimerize along the crystalline *a*-axis and form an array of quasi-1D metallic chains. Our finding suggests the use of WTe₂ for potential applications with respect to THz circular dichroism and characterization of chiral materials²⁸. For instance, the recently observed spontaneous gyrotropic electronic order in 1T-TiSe₂ allows one to induce chirality on demand using circularly polarized far-infrared light in the near field²⁹, and this should extend to a broader class of materials with energy gaps at THz frequencies. Our findings furthermore provide a new means for characterizing electromagnetic fields in the near field of materials, including possible hyperbolic responses.^{27,30} More broadly, this work demonstrates new possibilities for the development of ultrathin waveplates for on-chip two-dimensional opto-electronic applications at THz frequencies.³¹⁻³⁵

References:

- 1 Xia, F., Wang, H., Xiao, D., Dubey, M. & Ramasubramaniam, A. Two-dimensional material nanophotonics. *Nature Photonics* **8**, 899-907 (2014). https://doi.org/10.1038/nphoton.2014.271
- McIver, J. W., Hsieh, D., Steinberg, H., Jarillo-Herrero, P. & Gedik, N. Control over topological insulator photocurrents with light polarization. *Nature Nanotechnology* **7**, 96-100 (2011). https://doi.org/10.1038/nnano.2011.214

- Yang, H. *et al.* Optical Waveplates Based on Birefringence of Anisotropic Two-Dimensional Layered Materials. *ACS Photonics* **4**, 3023-3030 (2017). https://doi.org/10.1021/acsphotonics.7b00507
- 4 Mao, N. *et al.* Optical Anisotropy of Black Phosphorus in the Visible Regime. *J. Am. Chem. Soc.* 138, 300-305 (2016). https://doi.org/10.1021/jacs.5b10685
- Niu, S. *et al.* Giant optical anisotropy in a quasi-one-dimensional crystal. *Nature Photonics* **12**, 392-396 (2018). https://doi.org/10.1038/s41566-018-0189-1
- Ma, W. *et al.* In-plane anisotropic and ultra-low-loss polaritons in a natural van der Waals crystal. *Nature* **562**, 557-562 (2018). https://doi.org/10.1038/s41586-018-0618-9
- Folland, T. G. & Caldwell, J. D. Precise control of infrared polarization. *Nature* **562**, 499-501 (2018). https://doi.org/10.1038/d41586-018-07087-5
- Biswas, S., Grajower, M. Y., Watanabe, K., Taniguchi, T. & Atwater, H. A. Broadband electro-optic polarization conversion with atomically thin black phosphorus. *Science* **374**, 448-453 (2021). https://doi.org/10.1126/science.abj7053
- Zhang, H. *et al.* Cavity-enhanced linear dichroism in a van der Waals antiferromagnet. *Nature Photonics* **16**, 311-317 (2022). https://doi.org/10.1038/s41566-022-00970-8
- Mar, A., Jobic, S. & Ibers, J. A. Metal-metal vs tellurium-tellurium bonding in WTe₂ and its ternary variants TaIrTe₄ and NbIrTe₄. *J. Am. Chem. Soc.* **114**, 8963-8971 (1992). https://doi.org/10.1021/ja00049a029
- Ali, M. N. *et al.* Large, non-saturating magnetoresistance in WTe₂. *Nature* **514**, 205-208 (2014). https://doi.org/10.1038/nature13763
- Muscher, P. K. *et al.* Highly Efficient Uniaxial In-Plane Stretching of a 2D Material via Ion Insertion. *Advanced Materials* 33, 2101875 (2021). https://doi.org/https://doi.org/10.1002/adma.202101875
- Sie, E. J. *et al.* An ultrafast symmetry switch in a Weyl semimetal. *Nature* **565**, 61-66 (2019). https://doi.org/10.1038/s41586-018-0809-4
- Ofori-Okai, B. K. *et al.* A terahertz pump mega-electron-volt ultrafast electron diffraction probe apparatus at the SLAC Accelerator Structure Test Area facility. *J. Instrum.* **13**, P06014-P06014 (2018). https://doi.org/10.1088/1748-0221/13/06/p06014
- Li, R. K. *et al.* Terahertz-based subfemtosecond metrology of relativistic electron beams. *Phys. Rev. Accel. Beams* **22**, 012803 (2019). https://doi.org/10.1103/PhysRevAccelBeams.22.012803
- Baek, I. H. *et al.* Real-time ultrafast oscilloscope with a relativistic electron bunch train. *Nature Communications* **12**, 6851 (2021). https://doi.org/10.1038/s41467-021-27256-x
- Frühling, U. Light-field streaking for FELs. *J. Phys. B: At. Mol. Opt. Phys.* **44**, 243001 (2011). https://doi.org/10.1088/0953-4075/44/24/243001
- Curry, E., Fabbri, S., Maxson, J., Musumeci, P. & Gover, A. Meter-Scale Terahertz-Driven Acceleration of a Relativistic Beam. *Phys. Rev. Lett.* **120**, 094801 (2018). https://doi.org/10.1103/PhysRevLett.120.094801
- Othman, M. A. K. *et al.* Measurement of femtosecond dynamics of ultrafast electron beams through terahertz compression and time-stamping. *Applied Physics Letters* **122**, 141107 (2023). https://doi.org/10.1063/5.0134733
- Zhao, L. *et al.* Terahertz Oscilloscope for Recording Time Information of Ultrashort Electron Beams. *Phys. Rev. Lett.* **122**, 144801 (2019). https://doi.org/10.1103/PhysRevLett.122.144801
- Rakić, A. D., Djurišić, A. B., Elazar, J. M. & Majewski, M. L. Optical properties of metallic films for vertical-cavity optoelectronic devices. *Appl. Opt.* **37**, 5271 (1998). https://doi.org/10.1364/ao.37.005271
- Ordal, M. A. *et al.* Optical properties of the metals Al, Co, Cu, Au, Fe, Pb, Ni, Pd, Pt, Ag, Ti, and W in the infrared and far infrared. *Appl. Opt.* **22**, 1099 (1983). https://doi.org/10.1364/ao.22.001099
- Frenzel, A. J. *et al.* Anisotropic electrodynamics of type-II Weyl semimetal candidate WTe₂. *Phys. Rev. B* **95**, 245140 (2017). https://doi.org/10.1103/PhysRevB.95.245140

- Kimura, S.-i. *et al.* Optical evidence of the type-II Weyl semimetals ${\mathrm{MoTe}}_{2}$ and ${\mathrm{WTe}}_{2}$. *Physical Review B* **99**, 195203 (2019). https://doi.org/10.1103/PhysRevB.99.195203
- Homes, C. C., Ali, M. N. & Cava, R. J. Optical properties of the perfectly compensated semimetal WTe₂. *Phys. Rev. B* **92**, 161109 (2015). https://doi.org/10.1103/PhysRevB.92.161109
- Li, Y. & Heinz, T. F. Two-dimensional models for the optical response of thin films. *2D Materials* 5, 025021 (2018). https://doi.org/10.1088/2053-1583/aab0cf
- Wang, C. *et al.* Van der Waals thin films of WTe₂ for natural hyperbolic plasmonic surfaces. *Nature Communications* **11**, 1158 (2020). https://doi.org/10.1038/s41467-020-15001-9
- Narang, P., Garcia, C. A. C. & Felser, C. The topology of electronic band structures. *Nature Materials* (2020). https://doi.org/10.1038/s41563-020-00820-4
- 29 Xu, S. Y. *et al.* Spontaneous gyrotropic electronic order in a transition-metal dichalcogenide. *Nature* **578**, 545-549 (2020). https://doi.org/10.1038/s41586-020-2011-8
- Wang, H. & Low, T. Hyperbolicity in two-dimensional transition metal ditellurides induced by electronic bands nesting. *Physical Review B* **102**, 241104 (2020). https://doi.org/10.1103/PhysRevB.102.241104
- Gao, L. *et al.* On-chip plasmonic waveguide optical waveplate. *Sci. Rep.* **5**, 15794 (2015). https://doi.org/10.1038/srep15794
- Nouman, M. T., Hwang, J. H. & Jang, J. H. Ultrathin Terahertz Quarter-wave plate based on Split Ring Resonator and Wire Grating hybrid Metasurface. *Sci. Rep.* **6**, 39062 (2016). https://doi.org/10.1038/srep39062
- Zhao, Y. & Alù, A. Manipulating light polarization with ultrathin plasmonic metasurfaces. *Phys. Rev. B* **84**, 205428 (2011). https://doi.org/10.1103/PhysRevB.84.205428
- Yu, S., Wu, X., Wang, Y., Guo, X. & Tong, L. 2D Materials for Optical Modulation: Challenges and Opportunities. *Advanced Materials* **29**, 1606128 (2017). https://doi.org/https://doi.org/10.1002/adma.201606128
- Low, T. *et al.* Polaritons in layered two-dimensional materials. *Nature Materials* **16**, 182-194 (2017). https://doi.org/10.1038/nmat4792

Acknowledgments:

This work is supported primarily by the Department of Energy, Office of Basic Energy Sciences, Division of Materials Sciences and Engineering, under contract DE-AC02-76SF00515 (E.J.S., C.M.N., B.G., C.X., J.X., A.P., C.D.P., T.P.D., T.F.H., A.M.L.). E.J.S. acknowledges additional support from Stanford GLAM Postdoctoral Fellowship Program. C.M.N. acknowledges additional support from the NSF through a Graduate Research Fellowship (DGE-114747). T.F.H. acknowledges additional funding for analysis from the Gordon and Betty Moore Foundation EPiQS Initiative through Grant No. GBMF4545. S.J.P. is supported by the U.S. Department of Energy (DE-SC0012375). C.A.C.G., Y.W., and P.N. acknowledge support from the Department of Energy 'Photonics at Thermodynamic Limits' Energy Frontier Research Center under grant DE-SC0019140 (theoretical and computational approaches in light-matter interactions). C.A.C.G. acknowledges additional support from the NSF Graduate Research Fellowship Program under grant no. DGE-1745303. P.N. is a Moore Inventor Fellow and gratefully acknowledges support through Grant GBMF8048 from the Gordon and Betty Moore Foundation. B.K.O.-O. acknowledges support from the DOE Office of Science, Fusion Energy Science, under grant number FWP 100182. M.C.H. is supported by the U.S. Department of Energy, Office of Science,

Office of Basic Energy Sciences, under Award No. 2015-SLAC-100238-Funding. J.X. acknowledges additional support from the Office of Naval Research through Grant N00014-24-1-2068. X.W. acknowledges additional support by the Deutsche Forschungsgemeinschaft (DFG, German Research Foundation) - Project-ID 278162697 - SFB 1242. N.F. acknowledges the Stewardship Science Graduate Fellowship program's support, provided under cooperative agreement number DE-NA0002135. Sample synthesis and preparation were supported by the U.S. Department of Energy, DE-SC0016703 (D.R., J.H.). L.B. acknowledges support from the Office Naval Research through DURIP Grant No. 11997003 (transfer and stacking under inert conditions) and the National Science Foundation through DMR-1807969 (synthesis and student support). The National High Magnetic Field Laboratory is supported by National Science Foundation through NSF/DMR-1157490, NSF/DMR-1644779 and the State of Florida. First-principles calculations by C.D.P. were supported by the TIMES program at SLAC. This research used resources of the National Energy Research Scientific Computing Center (NERSC), a DOE Office of Science User Facility supported by the Office of Science of the U.S. Department of Energy under Contract No.DE-AC02-05CH11231. The experiment was performed at SLAC MeV-UED, which is supported in part by the DOE BES SUF Division Accelerator & Detector R&D program, the LCLS Facility, and SLAC under contract Nos. DE-AC02-05-CH11231 and DE-AC02-76SF00515. The authors thank Alex Frenzel, Alexey Belyanin, Dmitry Pikulin, Adolfo Grushin, and Roni Ilan for helpful discussions.

Competing interests:

The authors declare no competing financial interests.

Data availability:

The data that support the findings of this study are available from the corresponding author on reasonable request.

Supporting Information:

- 1. Materials and methods.
- 2. THz-streaking of electron beam
- 3. Sample dielectric environment and orientation with respect to Si frame edge
- 4. DFT calculations on phonons and interband optical excitations
- 5. Broadband nature of response
- 6. Birefringent response of transmitted field
- 7. Additional evidence of WTe₂ birefringence from a tabletop THz transmission
- 8. Electronic structure theory calculations on intraband transitions: Drude lifetimes, conductivity, and dielectric functions
- 9. Direct sampling using diffracted electron bean in UED
- 10. Modeling of transient streaking dynamics through interaction with a birefringent film Figures S1 to S17

Movies M1 to M4

- M1 THz streaking through a pinhole at increasing time delay
- M2 THz streaking through 50-nm thick WTe₂ with field polarized along a-axis
- M3 THz streaking through 50-nm thick WTe₂ with field polarized along b-axis
- M4 THz streaking through 50-nm thick WTe₂ with field polarized at 45 $^{\circ}$ from *a*-axis Supporting Information References

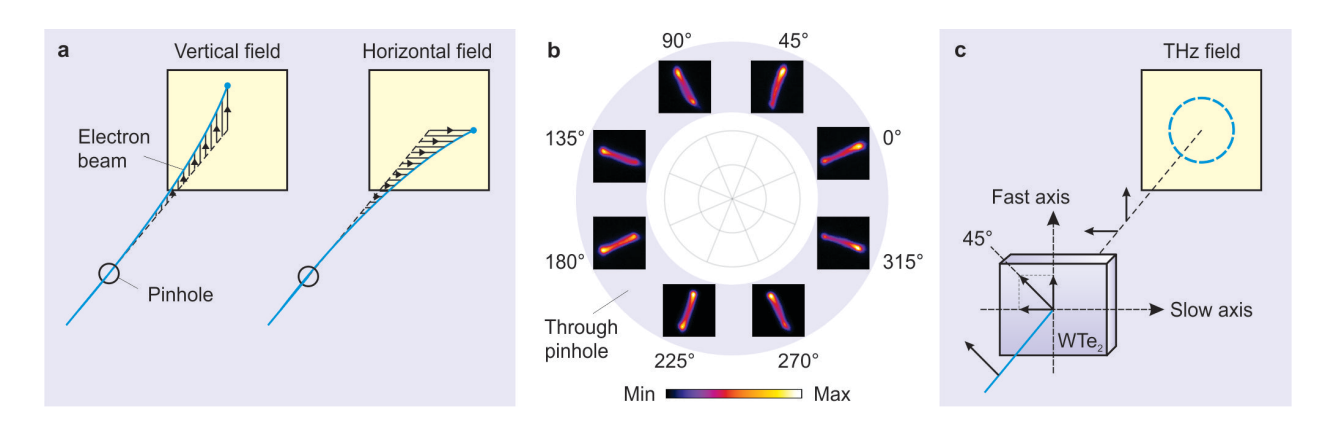


Figure 1. Streaking electrons using electric field from THz light pulses. (a) Electron beam is deflected along the vertical or horizontal direction depending on the electric field polarization. **(b)** Measured THz streaking of electron beams through a pinhole using THz light pulses at various linear polarization. **(c)** Schematic of circular streaking of electrons within a WTe₂ 50-nm thin film for a circularly polarized THz pulse in the near field.

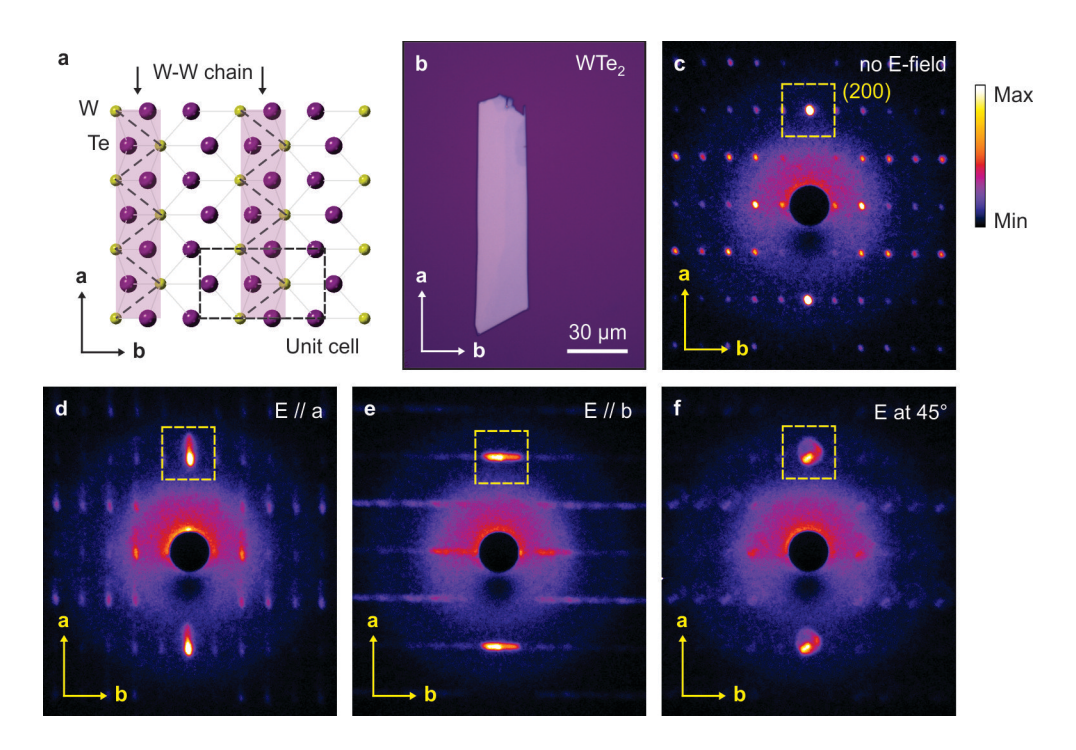


Figure 2. THz streaking nested in WTe₂ diffraction pattern. (a) Lattice structure of WTe₂ ab-plane. **(b)** Optical microscope image of an exfoliated 50-nm thick, 110 μ m \times 30 μ m WTe₂ sample on a SiO₂/Si substrate. **(c)** Measured electron diffraction pattern through WTe₂ with no applied THz E-field. **(d-f)** Measured electron diffraction pattern with THz E-field polarized along a-axis (d), along b-axis (e), and at 45° with respect to a and b axes (f).

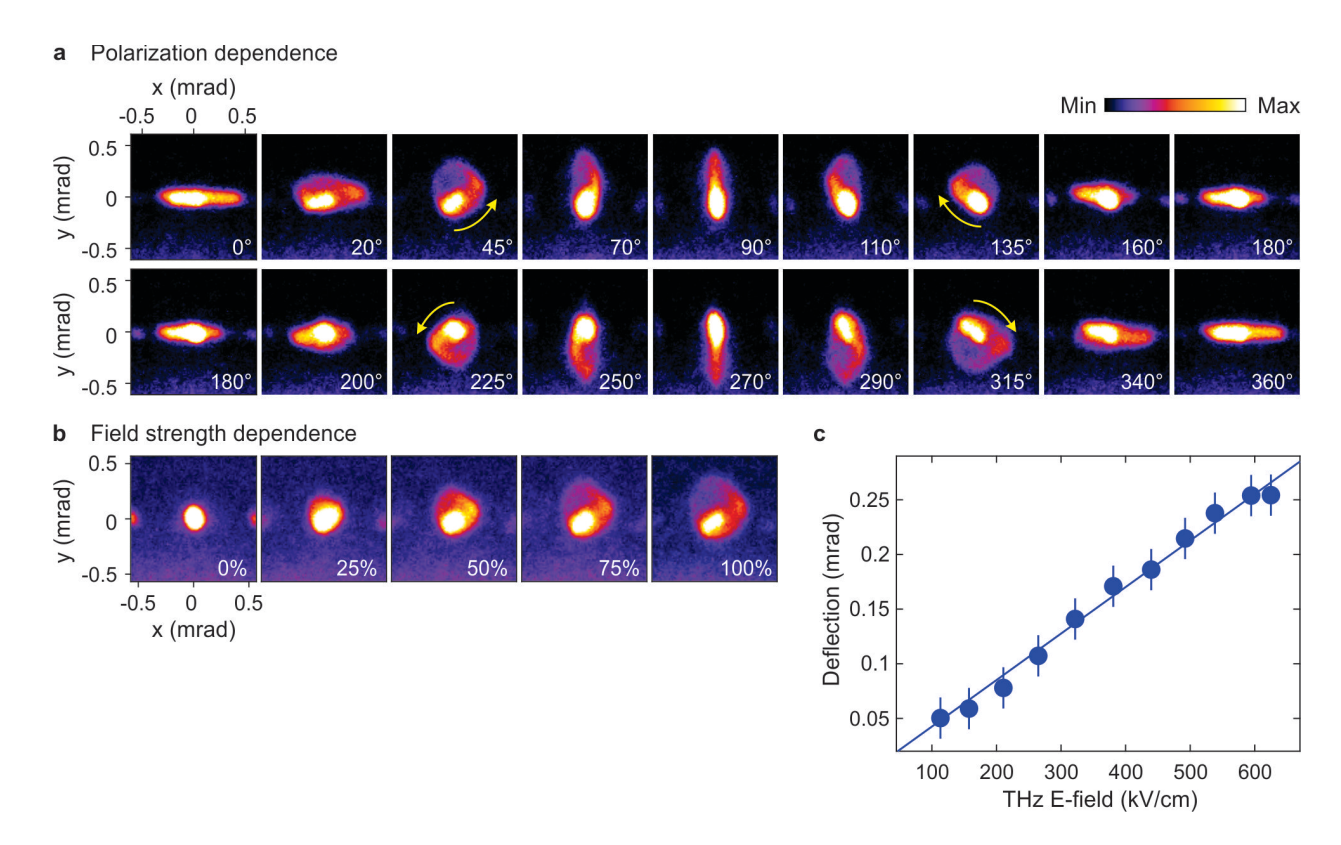


Figure 3. Polarization and field strength dependences of THz streaking. (a) Measured THz streaking at various incident THz polarizations through WTe₂. We obtained left-handed trajectories at 45° and 225°, and right-handed trajectories at 135° and 315°. (b) Measured electron streaking trajectory (45°) at increasing THz electric field strength up to a maximum of 625 kV/cm. (c) Measured electron deflection amplitude at increasing THz electric field strength shows a linear dependence. The vertical error bars represent standard deviations.

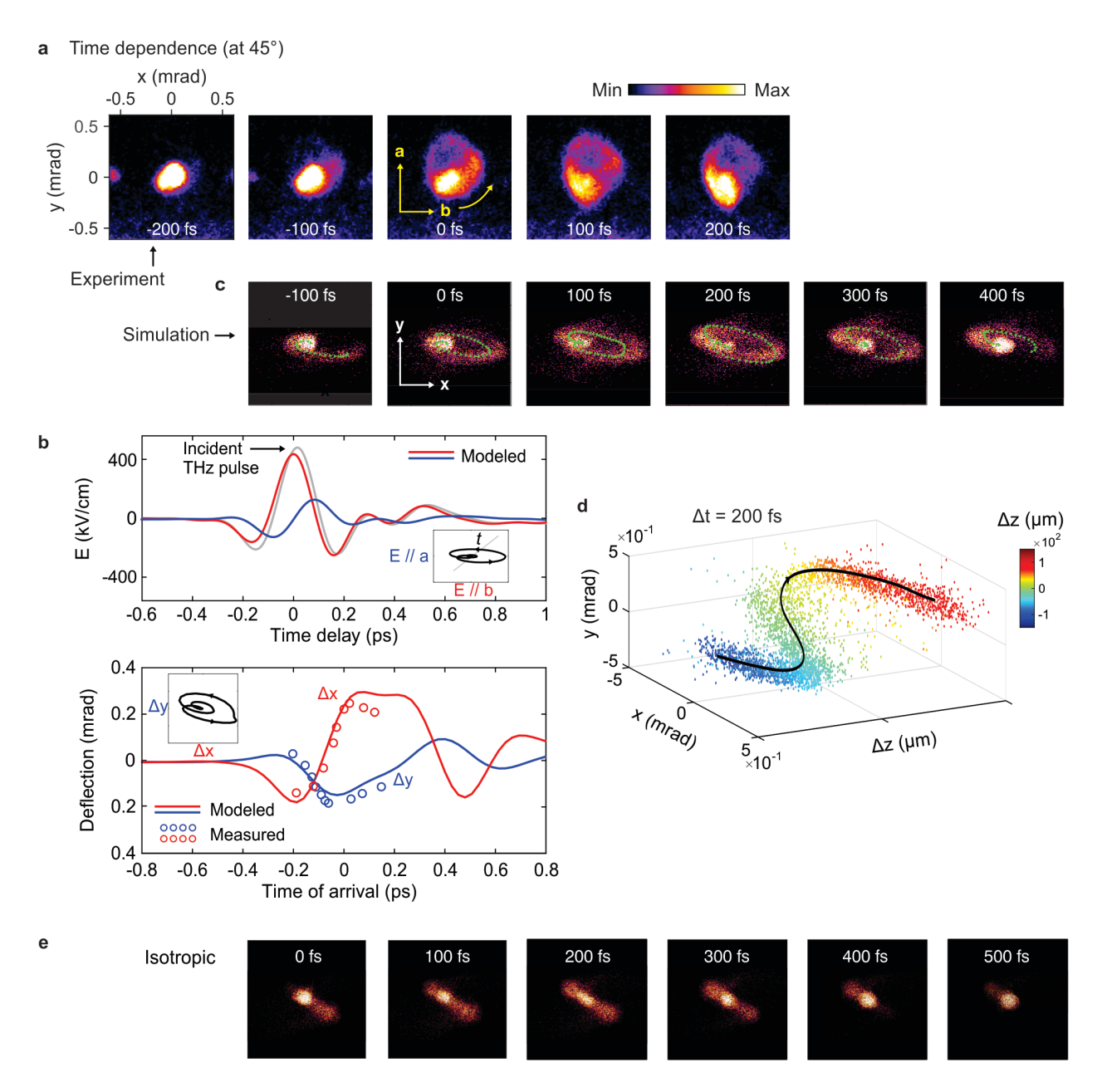


Figure 4. Capturing the THz trajectory motion in time. (a) Measured THz streaking at increasing time delay t between the electron bunch and the THz light pulse. The incident THz polarization is fixed at 45° with respect to a and b axes. **(b)** (top panel) THz time profile measured using EO-sampling (grey), and simulated fields within the sample (at z=0) decomposed along the in-plane a (vertical) and b (horizontal) axes, showing significant birefringence. (bottom panel) Simulated beam deflection at detector plane and decomposed into orthogonal components, as compared to data (extracted from measurements shown in a). **(c)** Modeled electron trajectory obtained from 3D simulations of the WTe₂ film interacting with the THz pulse in the near field, at z=0, at various time delays. **(d)** Simulated helical trajectory of electron in near field. **(e)** Simulations comparing assumed isotropic to anisotropic optical properties.

TOC Graphic

